

Strain-induced semiconductor to metal transition in MA_2Z_4 bilayers

Hongxia Zhong¹, Wenqi Xiong¹, Pengfei Lv¹, Jin Yu^{2,3*}, and Shengjun Yuan^{1*}

¹School of Physics and Technology, Wuhan University, Wuhan, 430072, People's Republic of China

²Institute for Molecules and Materials, Radboud University, Heijendaalseweg 135, NL-6525 AJ Nijmegen, The Netherlands

³School of Mechanics and Engineering Science, Shanghai University, Shanghai, 200444, China

Abstract

Very recently, a new type of two-dimensional layered material MoSi_2N_4 has been fabricated, which is semiconducting with weak interlayer interaction, high strength, and excellent stability. We systematically investigate theoretically the effect of vertical strain on the electronic structure of MA_2Z_4 ($\text{M}=\text{Ti}/\text{Cr}/\text{Mo}$, $\text{A}=\text{Si}$, $\text{Z}=\text{N}/\text{P}$) bilayers. Taking bilayer MoSi_2N_4 as an example, our first principle calculations show that its indirect band gap decreases monotonically as the vertical compressive strain increases. Under a critical strain around 22%, it undergoes a transition from semiconductor to metal. We attribute this to the opposite energy shift of states in different layers, which originates from the built-in electric field induced by the asymmetric charge transfer between two inner sublayers near the interface. Similar semiconductor to metal transitions are observed in other strained MA_2Z_4 bilayers, and the estimated critical pressures to realize such transitions are within the same order as semiconducting transition metal dichalcogenides. The semiconductor to metal transitions observed in the family of MA_2Z_4 bilayers present interesting possibilities for strain-induced engineering of their electronic properties.

Introduction

The family of two-dimensional (2D) materials is attracting great interest since the exfoliation of monolayer graphene from graphite.^{1, 2} They have many unique properties and distinguished performance for applications including mechanic engineering, electronics, information and energy technologies.³⁻⁸ Motivated by this, many new 2D materials have been continuously proposed by theorists with excellent physical or chemical properties.⁹⁻¹³ However, only few of them are synthesized successfully in monolayers,¹⁴⁻¹⁹ and they are mostly lamellar in their natural bulk forms, with the component layers assembled by weak van der Waals interaction.

Recently, the research enthusiasm has been extended to those 2D materials whose bulk forms are not layered in nature. A typical example is the hexagonal MXenes family, which has been fabricated by etching out the A layers from MAX materials.²⁰⁻²² In a very recent work, MoSi₂N₄, as a member of another new family of 2D molybdenum nitride,^{23, 24} was successfully grown by chemical vapor deposition method.²⁰ It is reported to be semiconducting with high strength and remarkable stability.²⁰ Since multilayer MoSi₂N₄ are stacked by very weak van der Waals interaction, they are structurally flexible and easy to deform. Meanwhile, it is known that this kind of deformation may modify the physical properties of layered 2D materials dramatically. For example, in AB-stacked bilayer graphene, applying a perpendicular electric field can induce a gap opening in the electronic structure, and a subsequent compression of the interlayer spacing can widen the field-induced band gap (a 10% compression enhances the gap by 80%).²⁵ Another example is layered MoS₂, which has been shown theoretically and experimentally that it undergoes a transition from semiconductor to metal with vertical pressure.^{26, 27} In general, decreasing the interlayer spacing may induce charge redistribution in layered 2D materials, it is therefore interesting and important to figure out whether the semiconducting layered MoSi₂N₄ and other members in the MA₂Z₄ (M=Ti/Cr/Mo, A=Si, Z=N/P) family are tunable under vertical strain.

In this work, we will study this problem theoretically from first-principle density-functional theory calculations. Indeed, we show that the compressive strain can serve as an effective tool to tailor the electronic properties of bilayer MoSi₂N₄. Importantly, a semiconductor to metal transition is observed when the vertical compressive strain reaches 22%. Such a

semiconductor to metal transition is a result of opposite energy shifts of states in two layers. The opposite energy shifts are further attributed to the enhanced interlayer interaction via asymmetric charge redistribution at the interface. We further investigate the threshold vertical compressive strain and estimate the corresponding pressure for MoSi₂N₄ and other semiconducting MA₂Z₄ bilayers. Our theoretical studies of their tunable electronic properties provide a guide for further experimental investigation, and bring opportunities to build novel electro-mechanical devices from these newly synthesized 2D materials.

Calculation method

Our calculations are performed using the projector augmented wave (PAW) method²⁸ implemented in the Vienna ab initio simulation package (VASP) code.²⁹ Perdew, Burke, and Ernzerhof (PBE) form of the generalized gradient approximation (GGA) exchange correlation functional³⁰ with van der Waals corrections (vdW-DFT),^{31, 32} and the PAW pseudo potentials²⁸ are adopted. The cut-off energy is set to 500 eV after convergence tests. A Γ -centered Monkhorst-Pack k -point grid^{33, 34} of $9 \times 9 \times 1$ is used for relaxations and the grid of $15 \times 15 \times 1$ for property calculations. In our current calculations, the total energy is converged to less than 10^{-6} eV, and the maximum force is less than 0.01 eV/Å during the optimization. A vacuum space along z -axis is larger than 20 Å to avoid spurious interactions. During the structure relaxation, the z coordinates of N atoms at the interface are fixed to ensure the layer spacing, and the z -axis is fixed to ensure the thickness of the vacuum slab. The spin-orbit coupling (SOC) have been examined for unstrained bilayer sheets.

Results and Discussions

We first perform calculations on monolayer MoSi₂N₄ and compare with reported results. The lattice constant is 2.91 Å, and the indirect band gap is 1.789 eV. They are in agreement with previous values of 2.94 Å and 1.744 eV, respectively.²⁰ With different stacking configurations, two MoSi₂N₄ monolayers can form three different bilayer structures (AA, AB and AC) with high symmetry.²⁰ Based on our calculated total energies, the order of stability of these three structures is AA < AB < AC. Hence, we take most stable AC stacking to discuss the related electronic properties in the rest of the paper.

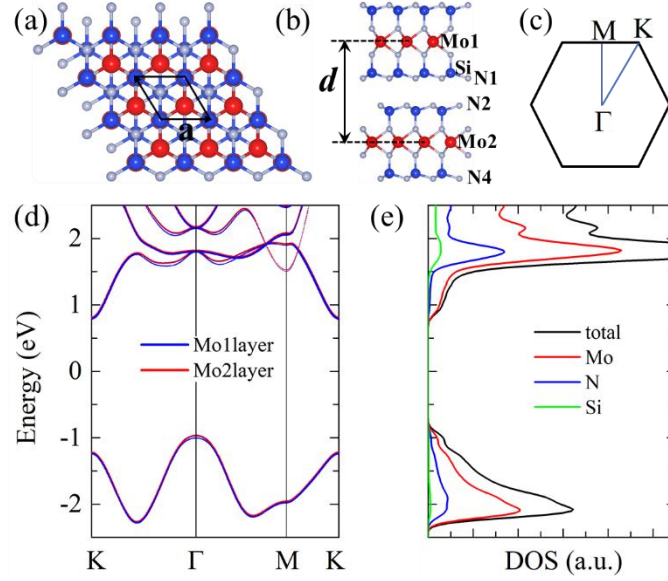


Fig. 1: Top (a) and side (b) views of atomic structure of bilayer MoSi_2N_4 . The primitive cell and lattice vector \mathbf{a} are indicated in (a). d is the interlayer distance between the top Mo1 and bottom Mo2 sublayers. (c) The first Brillouin zone of bilayer MoSi_2N_4 . Projected band structure (d) and partial density of states (e) of bilayer MoSi_2N_4 . The band gap center is set to be zero.

The ball-stick structures of AC-stacked MoSi_2N_4 are presented in Fig. 1. The unit cell and unit vectors are marked by black vectors. As shown in Figs. 1(a) and 1(b), the Si atoms of the top monolayer are superimposed on the Mo2 atom of the bottom monolayer, and the Mo1 atom of the top monolayer are superimposed on the N1 and N4 atoms of the bottom monolayer, i.e., sitting above the hexagon centers of the bottom lattice. The optimized lattice constant is 2.91 Å, which is the same as that of monolayer. The layer distance between Mo1 and Mo2 atoms is 11.030 Å, much larger than the one (6.23~ 6.54 Å) of bilayer transition metal dichalcogenides (TMDCs), such as MoS_2 , WS_2 , MoSe_2 and WSe_2 .^{35, 36} This suggests that the interlayer vdW interaction in bilayer MoSi_2N_4 will be much weaker than bilayer TMDCs. Such interlayer interaction is too weak so that the band structure of bilayer MoSi_2N_4 is almost the same as two isolated monolayers (as shown in Fig. 1(d)), except that there are negligible splittings of the highest (lowest) occupied (unoccupied) states along Γ -K and Γ -M directions. For bilayer MoSi_2N_4 , the valence band maximum (VBM) locates at Γ point, about 0.271 eV higher than the highest occupied states at K point, while the conduction band

minimum (CBM) is at K point, indicating an indirect band gap of 1.761 eV. If we include the spin-orbital coupling (SOC) in the calculations, there will be a band splitting (0.141 eV) of the highest occupied states at K point. This spin-induced splitting is compared to the value (0.149 eV) of MoS₂.^{37, 38} By contrast, no spin splitting is observed in the CBM at K point after including the SOC effects. In Fig. 1(e), the projected density of states indicates that both VBM and CBM are dominated by Mo atoms, with partly contributions from N atoms, but almost no contribution from Si atoms. By a more detailed analysis of the orbital contributions, the band edges are indeed mainly from the localized Mo dz^2 orbitals. It is worth to note that the observed SOC effects and orbital characters of the states at band edges are very similar to TMDC monolayers. Apart from the valence band splitting at K point, the SOC effect does not modify the band dispersion and band gap of bilayer MoSi₂N₄, and thus we will neglect it in the following sections.

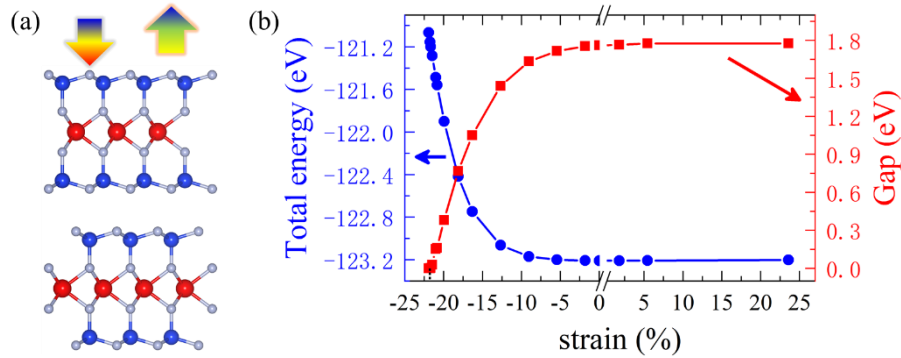


Fig 2: (a) Schematic diagram of the bilayer MoSi₂N₄ under an external vertical strain along the direction perpendicular to the layer, where the arrows pointing up and down represent a stretched and compressive strain, respectively. (b) The variation of total energy and band gap of bilayer MoSi₂N₄ as function of the interlayer spacing. The zero band gaps have been indicated by the black dotted line.

Applying vertical strain is an effective way to modulate the electronic properties of layered materials. It can be realized by hydrostatic pressure,³⁹ vacuum thermal annealing, nanomechanical pressures, or via inserting hexagonal BN dielectric layers.⁴⁰ In our calculations, the vertical strain is implemented by the change of the interlayer distance and characterized by a quantity $\delta = (d - d_0)/d_0$, where d and d_0 is the vertical distance for strained and unstrained bilayers. Fig. 2(a) shows schematic diagram of bilayer MoSi₂N₄ under vertical strain perpendicular to the plane of the layer, where the arrows pointing upward and

downward indicate a stretched and compressive strain, respectively. Fig. 2(b) depicts the evolutions of the total energy and band gap of bilayer MoSi₂N₄ under different vertical strains. For the intrinsic structure ($\delta = 0$), bilayer MoSi₂N₄ with interlayer distance 11.030 Å is the most stable configuration with the lowest total energy. Within the range $\delta \geq -0.09$, the total energy keeps almost the same, indicating that the interlayer interaction is too weak to affect the electronic properties. While for the vertical strain smaller than -0.09, i.e., a compressed strain more than 9%, the total energy increases monotonically with the decreasing vertical strain. Thus, the vertical strain with $\delta = -0.09$ can be regarded as the turning point where the interlayer interaction becomes so strong that cannot be neglected.

For the change of the band gap, when the value of δ is above the threshold -0.09, the indirect band gap is almost unchanged, similar to the property of total energy. When δ is below the threshold -0.09, the band gap decreases significantly. This threshold strain corresponds to a vertical distance of 3.02 Å between inner N atoms of two monolayers, which is comparable to the layer spacing of layered TMDCs,⁴¹ black phosphorene (3.21 Å),⁴² and borophene (3.07 Å).⁴³ In layered TMDCs, the interlayer interaction does affect their electronic structures greatly, changing the band gap from direct in monolayer to indirect in multilayers.^{19, 44, 45} Here, if we continuously increase the compressed strain in bilayer MoSi₂N₄, an electronic phase transition from semiconductor to metal is finally observed when the value of δ reaches -22%. The corresponding vertical compressive pressure P is 18.66 GPa, which is estimated in terms of $P = \frac{E - E_0}{(d_0 - d) * A}$,^{41, 46} where E and E_0 are total energies at the layer distance d and d_0 (equilibrium), and A is the area of the cell. Such a transition pressure is on the similar order of bilayer TMDCs (5.10-16.28 GPa).⁴¹ Generally, the electronic phase transition is accompanied by structural transition under high pressure.⁴⁷ While for bilayer MoSi₂N₄ under the transition pressure around 18.66 GPa, AC stacking is still found to be the most stable one, indicating that there will be no structural transition during the strain process. This is consistent with the excellent ambient stability observed in layered MoSi₂N₄.²⁰ Our predicted transition pressure of bilayer MoSi₂N₄ can be realized by hydrostatic pressure,³⁹ making it attractive for electro-mechanical applications.

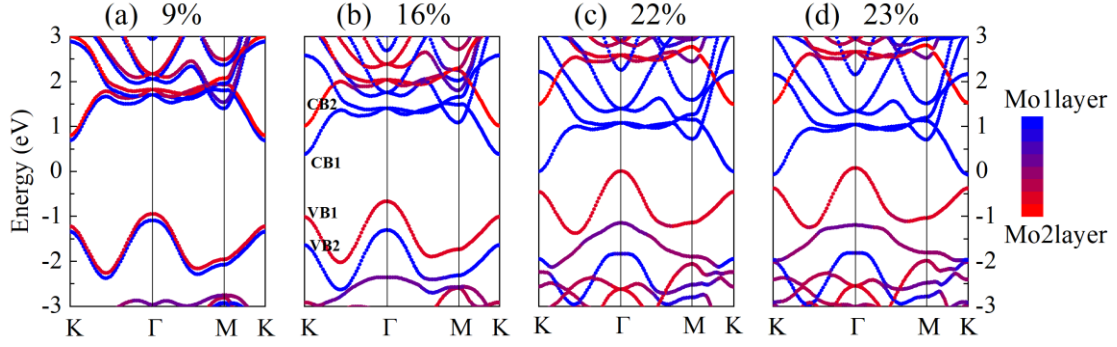


Fig 3: Band structures of bilayer MoSi_2N_4 under vertical compressive strains from 9% to 23%. All bands are shifted to align the deep Mo 4s state. Two conduction bands (CB1 and CB2) and two valence bands (VB1 and VB2) are labeled in (b).

Because the band gaps vary significantly within the range $\delta \leq -0.09$ in Fig. 2(b), we only focus on the vertical compressive strains in the following. In Fig. 3, we present the band structures of bilayer MoSi_2N_4 under four representative compressive strains from 9% to 23%. As the result of $\delta = 9\%$ shown in Fig. 3(a), notable changes appear in the electronic structure of bilayer MoSi_2N_4 that there are slight splittings of energy bands. These band splittings become more evident with the increasing of the compressive strain (see the changes of δ from 9% to 16% and 22%). Here, we can quantitatively define the rigid energy shift as the energy difference between the VB1 (CB1) and VB2 (CB2) at K (Γ) point as labeled in Fig. 3(b). When the compressive strain increases from 9% to 23%, the energy shift increases significantly from 0.116 to 1.605 eV. More importantly, the energy dispersion of each individual band keeps almost the same during the compression process. As a result, the charge carrier will maintain its small effective mass and high mobility ($270\text{-}1200 \text{ cm}^2 \text{ V}^{-1}\text{s}^{-1}$), similar as their values in pristine monolayer. If we inject electron or hole into a strained bilayer, crossing the energy band CB1 or VB1, then only the Mo1 layer or Mo2 layer will be conducting. Carrier injection thus can be used to effectively tune the transport properties of strained MoSi_2N_4 bilayers. It is also noted that the work function of bilayer MoSi_2N_4 is almost unchanged under different vertical strains. On the other hand, with the increasing compressive strain, both VBM and CBM are driven continuously toward the Fermi level, and thus reduce the energy band gap. The change of the band structure show that the indirect band gap of bilayer MoSi_2N_4 decreases from 1.633 to 0 eV, when the compressive strain increases from 9%

to 22%. After the compression reaches the critical value 22%, the metallic feature appears in the band structure as shown in Figs. 3(c) and 3(d) where $\delta \geq 22\%$, indicating clearly a robust semiconductor to metal phase transition.

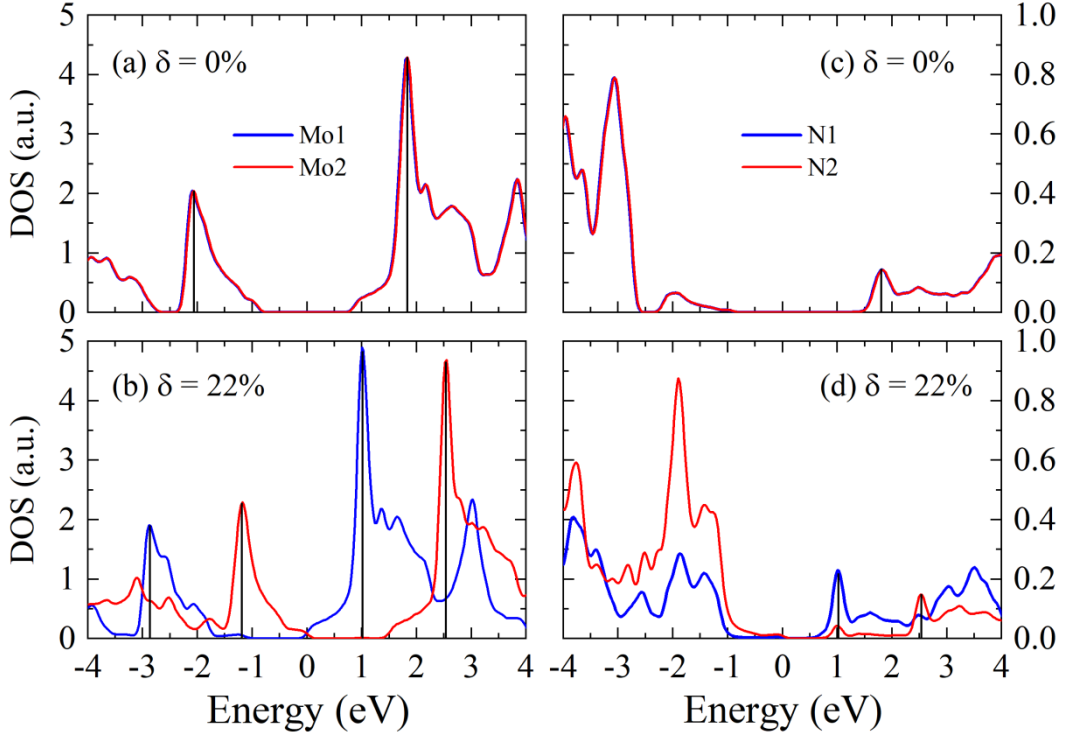


Fig 4: Partial density of states (PDOS) of Mo1, Mo2, N1 and N2 atoms (as labeled in Fig. 1) in bilayer MoSi_2N_4 with or without strain. All the energies are shifted to align the deep Mo 4s state.

In order to find the origin of this semiconductor to metal phase transition, we extract the partial density of states (PDOS) of bilayer MoSi_2N_4 with or without strain. As we have already shown that the band edges of bilayer MoSi_2N_4 are dominated by Mo states, we thus focus on the Mo states in two layers. In Fig. 4(a), the calculated PDOS of two Mo atoms from different layers in the pristine bilayer MoSi_2N_4 are totally degenerate, because of the symmetric atomic structures of the two layers. Under a vertical compressive strain 22%, the overall shape of the PDOS from two Mo are preserved but they have opposite energy shift, and there is an overlap of highest valence state of one Mo and the lowest conduction state of another Mo, as shown in Fig. 4(b). This overlap of Mo states agrees with the semiconductor to metal transition in bilayer MoSi_2N_4 under the critical strain of 22%. If we make an analysis

of the PDOS from N atoms in different layers, although their contributions to the states at the band edges are much smaller, the spectrum shift of each N atom is similar to the Mo atom within the same layer. Furthermore, there is a significant enhancement of PDOS of N1 and N2 atoms, indicating that there is an enhancement of interlayer interactions between the p_z orbitals of N atoms crossing the interface of the two layers.

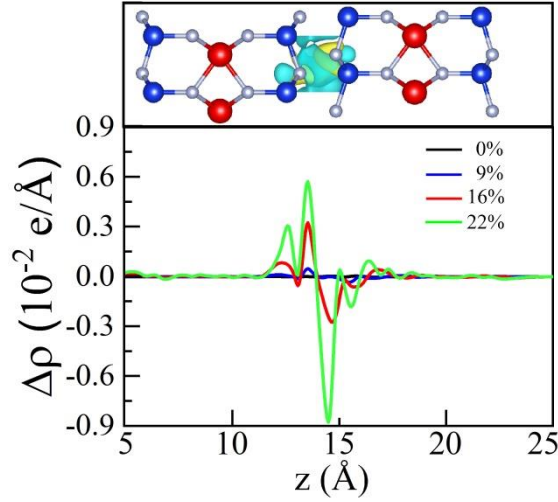


Fig 5: Plane-averaged charge density difference $\Delta\rho(z)$ of bilayer MoSi_2N_4 under vertical compressive strain from 0% to 22%. The top panel is a three-dimensional charge density difference under the strain 22%, and the isosurface value is $0.002 \text{ e}/\text{\AA}^3$. The green and yellow areas represent electron accumulation and depletion, respectively.

The opposite energy shift of the PDOS indicates a possible strain induced change of the electric potentials on these atoms. We thus calculate the plane-averaged charge density difference $\Delta\rho(z)$ along the vertical direction (z -axis) for MoSi_2N_4 bilayers with different strain and plot the results in Fig. 5. Here, $\Delta\rho(z)$ is calculated by the charge density difference between bilayer and two non-interacting monolayers. A positive $\Delta\rho(z)$ indicates the accumulating of the charge density, while a negative value means the depletion. For unstrained bilayer MoSi_2N_4 , $\Delta\rho(z)$ is almost zero for all z coordinates, suggesting no charge transfer between layers. This is also consistent with the observed very weak interlayer vdW interaction in pristine bilayer MoSi_2N_4 . For strained bilayer MoSi_2N_4 , we see clearly changes of $\Delta\rho(z)$ are totally different on the two sides of the interface. Although on both layers, there are fluctuations of $\Delta\rho(z)$, but clearly on one side the overall values of $\Delta\rho(z)$ are negative, and on the other side they are positive, indicating the charge transfer between the two layers. The

amount of charge transfer Q , obtained by the integral of $\Delta\rho(z)$ along one side of the interface, increase monotonically with the strain. Furthermore, if we calculate the ratio of $Q/\Delta\text{gap}$ for different strain, we obtain a similar value of 0.035. This correlation between Q and reduced energy gap indicate that, the asymmetric charge redistribution at the interface causes the opposite energy shift of the two layers, and subsequently the semiconductor to metal phase transition at the critical compressive strain.

Table 1. Distance between two Z atoms from different layers in pristine bilayer MA_4Z_2 or with a critical strain, and estimated pressure required for realizing the semiconductor to metal transition. We also list the vertical separation between interlayer anion atoms and the corresponding pressure for semiconductor to metal transition in some AB-stacked TMDCs for comparison.⁴¹

	Bilayer separation at transition (Å)	Bilayer separation at equilibrium (Å)	Transition pressure (GPa)
MoSi_2N_4	1.62	4.02	18.66
MoSi_2P_4	2.42	4.02	2.38
CrSi_2N_4	2.62	4.03	2.18
TiSi_2N_4	1.20	4.04	32.04
MoS_2	2.14	3.11	8.52
MoSe_2	2.23	3.19	8.37
MoTe_2	2.69	3.37	5.10
WS_2	1.80	3.39	16.28
WSe_2	2.21	3.35	15.83

To complete our study, we studied numerically the strain-induced semiconductor to metal transition in other MA_2Z_4 bilayers, and summarize their structural parameters and transition pressures in Table 1. Owing to the weak interlayer interaction, the interlayer separation for the unstrained bilayer MA_2Z_4 is all around 4.02 Å, larger than those (3.11-3.39 Å) of bilayer TMDCs.⁴¹ By increasing the vertical compressive strain, the interlayer separation decreases accordingly. Under the transition strain, all considered MA_2Z_4 bilayers change from semiconductor to metal t, and the interlayer separation ranges from 1.62 to 2.62 Å, similar to the range (1.80-2.69 Å) of bilayer TMDCs at the transition point.⁴¹ The estimated transition pressure ranges from 2.18 GPa in bilayer CrSi_2N_4 to 18.66 GPa in bilayer MoSi_2N_4 , which is

on the same order of that (5.10-19 GPa) of well-studied layered TMDCs.^{41, 47}. In particular, bilayer CrSi_2N_4 and MoSi_2P_4 , have very smaller transition pressures (2.18 - 2.38 GPa) comparing to other studied MA_2Z_4 . Our calculations suggest that the strain-induced semiconductor to metal transition in semiconducting bilayer MA_2Z_4 can be easily realized experimentally. Furthermore, our extended calculations show that semiconductor to metal transition also appears in four-layer MoSi_2N_4 , and the transition strain is around 18%, corresponding to 15.03GPa, which is smaller than that of stacked bilayer. Therefore,, we expect that similar transition can be observed in all multilayer and bulk MA_2Z_4 with experimentally reachable pressure.

Conclusion

In conclusion, we have studied the electronic properties of MA_2Z_4 ($\text{M}=\text{Ti}/\text{Cr}/\text{Mo}$, $\text{A}=\text{Si}$, $\text{Z}=\text{N}/\text{P}$) bilayers under different vertical strains using first-principle density-functional theory calculations. Taking the recently fabricated MoSi_2N_4 as an example, our results reveal that the electronic properties of bilayer MoSi_2N_4 can be effectively tuned by the vertical compressive strain. To be more exact, with an increasing compressive strain, the band gap of bilayer MoSi_2N_4 monotonically decreases and finally close when the vertical strain reaches 22%. This is a result of the opposite energy shift of the states in different layers, which is driven by the asymmetric charge redistribution on the inner A-A sublayer at the interface. We further conformed that similar semiconductor to metal transitions exists in other strained MA_2Z_4 bilayers, and the estimated transition pressure to realize such transition ranges from 2.18 GPa in CrSi_2N_4 to 32.04 GPa in TiSi_2N_4 . Our theoretical predictions provide a guiding for further exploring the strain-tunable electronic properties of layered semiconducting MA_2Z_4 .

Acknowledgement

This work is supported by the National Key R&D Program of China (Grant No.2018YFA0305800) and National Natural Science Foundation of China (Grant No. 11947218). Hongxia Zhong acknowledges the support by the China Postdoctoral Science Foundation (Grant No.2018M640723). Numerical calculations presented in this paper have

been performed on a supercomputing system in the Supercomputing Center of Wuhan University.

References

1. Novoselov, K. S.; Geim, A. K.; Morozov, S. V.; Jiang, D.; Zhang, Y.; Dubonos, S. V.; Grigorieva, I. V.; Firsov, A. A., Electric field effect in atomically thin carbon films. *Science* **2004**, *306* (5696), 666-669.
2. Novoselov, K. S.; Jiang, D.; Schedin, F.; Booth, T.; Khotkevich, V.; Morozov, S.; Geim, A. K., Two-dimensional atomic crystals. *PNAS* **2005**, *102* (30), 10451-10453.
3. Novoselov, K. S.; Geim, A. K.; Morozov, S. V.; Jiang, D.; Katsnelson, M. I., Two-dimensional gas of massless Dirac fermions in graphene. *Nature* **2005**, *438*, 197-200.
4. Novoselov, K. S.; Geim, A. K., The rise of graphene. *Nature Materials* **2007**, *6* (3), 183-191.
5. Novoselov, K. S.; Jiang, Z.; Zhang, Y.; Morozov, S.; Stormer, H. L.; Zeitler, U.; Maan, J.; Boebinger, G.; Kim, P.; Geim, A. K., Room-temperature quantum Hall effect in graphene. *Science* **2007**, *315* (5817), 1379-1379.
6. Pedersen, T. G.; Flindt, C.; Pedersen, J.; Mortensen, N. A.; Jauho, A.-P.; Pedersen, K., Graphene antidot lattices: designed defects and spin qubits. *Physical Review Letters* **2008**, *100* (13), 136804.
7. Zhang, Y.; Tan, Y.-W.; Stormer, H. L.; Kim, P., Experimental observation of the quantum Hall effect and Berry's phase in graphene. *Nature* **2005**, *438* (7065), 201-204.
8. Zhou, S. Y.; Gweon, G.-H.; Fedorov, A.; First, P., de; De Heer, W.; Lee, D.-H.; Guinea, F.; Neto, A. C.; Lanzara, A., Substrate-induced bandgap opening in epitaxial graphene. *Nature Materials* **2007**, *6* (10), 770-775.
9. Ataca, C.; Sahin, H.; Ciraci, S., Stable, single-layer MX₂ transition-metal oxides and dichalcogenides in a honeycomb-like structure. *The Journal of Physical Chemistry C* **2012**, *116* (16), 8983-8999.
10. Wu, W.; Lu, P.; Zhang, Z.; Guo, W., Electronic and magnetic properties and structural stability of BeO sheet and nanoribbons. *ACS Applied Materials & Interfaces* **2011**, *3* (12), 4787-4795.
11. Yu, J.; Guo, W., Two-dimensional hexagonal beryllium sulfide crystal. *The Journal of Physical Chemistry Letters* **2013**, *4* (11), 1856-1860.
12. Zhang, Z.; Liu, X.; Yakobson, B. I.; Guo, W., Two-dimensional tetragonal TiC monolayer sheet and nanoribbons. *Journal of the American Chemical Society* **2012**, *134* (47), 19326-19329.
13. Zhuang, H. L.; Hennig, R. G., Electronic structures of single-layer boron pnictides. *Applied Physics Letters* **2012**, *101* (15), 153109.
14. Chhowalla, M.; Shin, H. S.; Eda, G.; Li, L.-J.; Loh, K. P.; Zhang, H., The chemistry of two-dimensional layered transition metal dichalcogenide nanosheets. *Nature Chemistry* **2013**, *5* (4), 263-275.

15. Dean, C. R.; Young, A. F.; Meric, I.; Lee, C.; Wang, L.; Sorgenfrei, S.; Watanabe, K.; Taniguchi, T.; Kim, P.; Shepard, K. L., Boron nitride substrates for high-quality graphene electronics. *Nature Nanotechnology* **2010**, *5* (10), 722-726.
16. Ganatra, R.; Zhang, Q., Few-layer MoS₂: a promising layered semiconductor. *ACS Nano* **2014**, *8* (5), 4074-4099.
17. Li, L.; Yu, Y.; Ye, G. J.; Ge, Q.; Ou, X.; Wu, H.; Feng, D.; Chen, X. H.; Zhang, Y., Black phosphorus field-effect transistors. *Nature Nanotechnology* **2014**, *9* (5), 372.
18. Lu, G.; Wu, T.; Yuan, Q.; Wang, H.; Wang, H.; Ding, F.; Xie, X.; Jiang, M., Synthesis of large single-crystal hexagonal boron nitride grains on Cu–Ni alloy. *Nature Communications* **2015**, *6* (1), 1-7.
19. Mak, K. F.; Lee, C.; Hone, J.; Shan, J.; Heinz, T. F., Atomically thin MoS₂: a new direct-gap semiconductor. *Physical Review Letters* **2010**, *105* (13), 136805.
20. Hong, Y. L.; Liu, Z.; Wang, L.; Zhou, T.; Ren, W., Chemical vapor deposition of layered two-dimensional MoSi₂N₄ materials. *Science* **2020**, *369* (6504), 670-674.
21. Naguib, M.; Mochalin, V. N.; Barsoum, M. W.; Gogotsi, Y., 25th anniversary article: MXenes: a new family of two-dimensional materials. *Advanced Materials* **2014**, *26* (7), 992-1005.
22. Zhang, X.; Ma, Z.; Zhao, X.; Tang, Q.; Zhou, Z., Computational studies on structural and electronic properties of functionalized MXene monolayers and nanotubes. *Journal of Materials Chemistry A* **2015**, *3* (9), 4960-4966.
23. Xu, C.; Wang, L.; Liu, Z.; Chen, L.; Guo, J.; Kang, N.; Ma, X.-L.; Cheng, H.-M.; Ren, W., Large-area high-quality 2D ultrathin Mo₂C superconducting crystals. *Nature Materials* **2015**, *14* (11), 1135-1141.
24. Wang, Z.; Kochat, V.; Pandey, P.; Kashyap, S.; Chattopadhyay, S.; Samanta, A.; Sarkar, S.; Manimunda, P.; Zhang, X.; Asif, S., Metal immiscibility route to synthesis of ultrathin carbides, borides, and nitrides. *Advanced Materials* **2017**, *29* (29), 1700364.
25. Guo, Y.; Guo, W.; Chen, C., Tuning field-induced energy gap of bilayer graphene via interlayer spacing. *Applied Physics Letters* **2008**, *92* (24), 243101.
26. Nayak, A. P.; Bhattacharyya, S.; Zhu, J.; Liu, J.; Wu, X.; Pandey, T.; Jin, C.; Singh, A. K.; Akinwande, D.; Lin, J.-F., Pressure-induced semiconducting to metallic transition in multilayered molybdenum disulphide. *Nature Communications* **2014**, *5* (1), 1-9.
27. Chi, Z.-H.; Zhao, X.-M.; Zhang, H.; Goncharov, A. F.; Lobanov, S. S.; Kagayama, T.; Sakata, M.; Chen, X.-J., Pressure-induced metallization of molybdenum disulfide. *Physical Review Letters* **2014**, *113* (3), 036802.
28. Blöchl, P. E., Projector augmented-wave method. *Physical Review B* **1994**, *50* (24), 17953.
29. Kresse, G.; Furthmüller, J., Efficient iterative schemes for ab initio total-energy calculations using a plane-wave basis set. *Physical Review B* **1996**, *54* (16), 11169.
30. Perdew, J. P.; Burke, K.; Ernzerhof, M., Generalized Gradient Approximation Made Simple. *Physical Review Letters* **1996**, *77* (18), 3865-3868.
31. Klimeš, J.; Bowler, D. R.; Michaelides, A., Van der Waals density functionals

- applied to solids. *Physical Review B* **2011**, 83 (19), 195131.
32. Dion, M.; Rydberg, H.; Schröder, E.; Langreth, D. C.; Lundqvist, B. I., Van der Waals Density Functional for General Geometries. *Physical Review Letters* **2004**, 92 (24), 246401.
 33. Pack, J. D.; Monkhorst, H. J., "Special points for Brillouin-zone integrations"---a reply. *Physical Review B* **1977**, 16 (4), 1748-1749.
 34. Monkhorst, H. J.; Pack, J. D., Special points for Brillouin-zone integrations. *Physical Review B* **1976**, 13 (12), 5188-5192.
 35. Gao, S.; Yang, L.; Spataru, C. D., Interlayer coupling and gate-tunable excitons in transition metal dichalcogenide heterostructures. *Nano Letters* **2017**, 17 (12), 7809-7813.
 36. He, J.; Hummer, K.; Franchini, C., Stacking effects on the electronic and optical properties of bilayer transition metal dichalcogenides MoS₂, MoSe₂, WS₂, WSe₂. *Physical Review B* **2014**, 89 (7), 075409.
 37. Di, X.; Gui-Bin, L.; Wanxiang, F.; Xiaodong, X.; Wang, Y., Coupled Spin and Valley Physics in Monolayers of MoS₂ and Other Group-VI Dichalcogenides *Physical Review Letters* **2012**, 108, 196802.
 38. Wang, Y.; Deng, L.; Wei, Q.; Wan, Y.; Liu, Z.; Lu, X.; Li, Y.; Bi, L.; Zhang, L.; Lu, H., Spin-Valley Locking Effect in Defect States of Monolayer MoS₂. *Nano Letters* **2020**, 20 (3), 2129-2136.
 39. Fu, L.; Wan, Y.; Tang, N.; Ding, Y.-m.; Gao, J.; Yu, J.; Guan, H.; Zhang, K.; Wang, W.; Zhang, C., K-Λ crossover transition in the conduction band of monolayer MoS₂ under hydrostatic pressure. *Science Advances* **2017**, 3 (11), e1700162.
 40. Pham, K. D.; Hieu, N. N.; Phuc, H. V.; Fedorov, I.; Duque, C.; Amin, B.; Nguyen, C. V., Layered graphene/GaS van der Waals heterostructure: Controlling the electronic properties and Schottky barrier by vertical strain. *Applied Physics Letters* **2018**, 113 (17), 171605.
 41. Bhattacharyya, S.; Singh, A. K., Semiconductor-metal transition in semiconducting bilayer sheets of transition-metal dichalcogenides. *Physical Review B* **2012**, 86 (7), 075454.
 42. Fei, R.; Yang, L., Strain-engineering the anisotropic electrical conductance of few-layer black phosphorus. *Nano Letters* **2014**, 14 (5), 2884-2889.
 43. Zhong, H.; Huang, K.; Yu, G.; Yuan, S., Electronic and mechanical properties of few-layer borophene. *Physical Review B* **2018**, 98 (5), 054104.
 44. Splendiani, A.; Sun, L.; Zhang, Y.; Li, T.; Kim, J.; Chim, C.-Y.; Galli, G.; Wang, F., Emerging photoluminescence in monolayer MoS₂. *Nano Letters* **2010**, 10 (4), 1271-1275.
 45. Zhang, Y.; Chang, T.-R.; Zhou, B.; Cui, Y.-T.; Yan, H.; Liu, Z.; Schmitt, F.; Lee, J.; Moore, R.; Chen, Y., Direct observation of the transition from indirect to direct bandgap in atomically thin epitaxial MoSe₂. *Nature Nanotechnology* **2014**, 9 (2), 111.
 46. Gan, L.-Y.; Zhang, Q.; Cheng, Y.; Schwingenschlögl, U., Two-dimensional ferromagnet/semiconductor transition metal dichalcogenide contacts: p-type Schottky

- barrier and spin-injection control. *Physical Review B* **2013**, 88 (23), 235310.
47. Nayak, A. P.; Bhattacharyya, S.; Zhu, J.; Liu, J.; Wu, X.; Pandey, T.; Jin, C.; Singh, A. K.; Akinwande, D.; Lin, J.-F., Pressure-induced semiconducting to metallic transition in multilayered molybdenum disulphide. *Nature Communications* **2014**, 5 (1), 3731.